

The Dusty Starburst Nucleus of M33¹

Karl D. Gordon^{2,3}, M. M. Hanson^{4,5,6}, Geoffrey C. Clayton^{2,3,7}, G. H. Rieke⁴, and K. A. Misselt^{2,7}

ABSTRACT

We have thoroughly characterized the ultraviolet to near-infrared (0.15 - 2.2 μm) spectral energy distribution (SED) of the central parsec of the M33 nucleus through new infrared photometry and optical/near-infrared spectroscopy, combined with ultraviolet/optical observations from the literature and the HST archive. The SED shows evidence for a significant level of attenuation, which we model through a Monte Carlo radiative transfer code as a shell of clumpy Milky Way-type dust ($\tau_V \sim 2 \pm 1$). The discovery of Milky Way-type dust (with a strong 2175 \AA bump) internal to the M33 nucleus is different from previous work which has found SMC-like dust (no bump) near starburst regions. The amount by which dust can be processed may be related to the mass and age of the starburst as well as the extent to which the dust can shield itself. Our starburst models include the effects of this dust and can fit the SED if the nucleus was the site of a moderate ($\sim 10^8 L_\odot$ at 10 Myrs) episode of coeval star formation about 70 Myrs ago. This result is quite different from previous studies which resorted to multiple stellar populations (between 2 and 7) attenuated by either no or very little internal dust. The M33 nuclear starburst is remarkably similar to an older version (70 Myr versus 10 Myr) of the ultra-compact starburst in the center of the Milky Way.

Subject headings: galaxies: individual (M33) – galaxies: ISM – galaxies: starburst

¹Based on observations made with the NASA/ESA Hubble Space Telescope, obtained from the data Archive at the Space Telescope Science Institute, which is operated by the Association of Universities for Research in Astronomy, Inc., under NASA contract NAS5-26555.

²Department of Physics & Astronomy, Louisiana State University, Baton Rouge, LA 70803

³Visiting Astronomer at the Infrared Telescope Facility, which is operated by the University of Hawaii under contract from the National Aeronautics and Space Administration

⁴Steward Observatory, University of Arizona, Tucson, AZ 85721

⁵present address: Department of Physics, University of Cincinnati, Cincinnati, OH 45221

⁶Hubble Fellow

⁷Visiting Astronomer, Kitt Peak National Observatory, National Optical Astronomy Observatories, which is operated by the Association of Universities for Research in Astronomy, Inc. (AURA) under cooperative agreement with the National Science Foundation.

1. Introduction

The nucleus of M33 (NGC 598, Triangulum galaxy) has been studied extensively, but its true nature has remained elusive. It is bright and compact, has a FWHM of $0''.16$ ($= 0.6$ pc) in HST F555W observations, and lacks a substantial black hole (Kormendy & McClure 1993; Massey et al. 1996; Lauer et al. 1998). Van den Bergh (1991) reviews studies on the stellar populations in M33, including the nucleus. Previous work has found that the nucleus is composed of roughly two stellar populations, one with an age of $10^7 - 10^8$ years and one with an age of $10^9 - 10^{10}$ years (O’Connell 1983; Ciani, D’Odorico, & Benvenuti 1984; Schmidt et al. 1990).

Previous attempts at modeling the stellar population of the M33 nucleus have either ignored the effects of reddening internal to M33 or modeled it assuming a simple screen of dust. The presence of ultraviolet (UV) (especially far-UV [Massey et al. 1996]) flux from the M33 nucleus, and its small size, imply a coeval, young stellar population. The flat UV/optical spectrum of the M33 nucleus [Figure 1c of McQuade, Calzetti, & Kinney (1995)], when coupled with the assumption of a single young stellar population, can only be explained by significant reddening by dust internal to M33 (Calzetti et al. 1994). The work of Witt, Thronson, & Capuano (1992) demonstrates the importance of accurately treating the radiative transfer through the dust in galaxies.

The M33 nucleus is ideal for investigating the role of dust in starburst galaxies. Previous work on starburst galaxies found that the extinction curve lacks a 2175 \AA bump (Calzetti et al. 1994; Gordon et al. 1997). The only other dust which does not have a 2175 \AA bump is found in the Small Magellanic Cloud (SMC). Gordon & Clayton (1998) reinvestigated the UV extinction in the SMC and found evidence to support the processing of dust near sites of active star formation. Dust with weak 2175 \AA bumps is seen along some Galactic and Large Magellanic Cloud (LMC) sightlines (e.g. Cardelli & Savage 1988; Misselt, Clayton, & Gordon 1998). It is possible that the lack of a 2175 \AA bump is the result of processing the dust near sites of active star formation. The work of Gordon et al. (1997) was based on an IUE selected sample of starburst galaxies and due to the large aperture of IUE, the sample was observationally biased toward intrinsically bright starbursts with small amounts of dust. We probe the M33 nucleus with a model including stars, gas, and dust. We find that its dust has a strong 2175 \AA bump, in contrast to the behavior of the starburst dust studied previously (Gordon et al. 1997). This paper represents the beginning of a series of papers devoted to understanding the role of dust on the interpretation of stellar populations in starburst galaxies.

In this paper, we find that the M33 SED can be modeled as a modest ($\sim 7 \times 10^5 M_{\odot}$) ~ 70 Myr old starburst enshrouded by a shell of MW-like dust ($\tau_V \sim 2$) by using a starburst model which includes stars, gas, and dust. The indication of a young, very compact, and moderate luminosity starburst in the central pc of M33 is interesting because of the possible similarity to the very young and massive stars within the central 0.5 pc of the Milky Way. Because of their modest outputs and small sizes, such systems would not stand out clearly in the nuclei of galaxies

outside the Local Group. The presence of two similar events in Local Group galaxies suggests that such starbursts may be relatively common and hence may play an important role in the evolution of the central parsec-sized regions of galaxies.

2. Data

The observations of the M33 nucleus can be divided into two groups; photometry and spectroscopy. For photometric measurements, the background level is determined using an annulus surrounding the nucleus. As a result, the photometry of the M33 nucleus does not include a significant contribution from the disk or bulge of M33. The background levels for spectroscopic observations are usually measured a significant distance from the nucleus. This means they include contributions from regions surrounding the nucleus, which makes studying just the nucleus difficult. Thus, to isolate the spectral behavior of the nucleus requires a judicious combination of both photometry and spectroscopy.

2.1. Photometry

The Ultraviolet Imaging Telescope (UIT, Stecher et al. 1997) observed M33 during the Astro-1 mission in the far-UV (B1 filter, $\lambda_c \approx 1500 \text{ \AA}$) and the near-UV (A1 filter, $\lambda_c \approx 2400 \text{ \AA}$). The UIT images, along with ground-based UVB images, were analyzed by Massey et al. (1996). They present UIT-B1, UIT-A1, U, B, and V measurements of the nucleus of M33 (see Table 1) and note the nucleus is very red compared to the other sources in their images. Additional ground-based measurements at B and R are given by Kormendy & McClure (1993). The zero points for the U, B, V, and R magnitudes were taken from Bessell, Castelli, & Plez (1998).

Numerous WFPC2 images of the central region of M33 exist in the HST archive. We chose post-COSTAR images taken with at least two images in each filter to facilitate the removal of cosmic rays. The names, filters, and exposure times of the images used are listed in Table 2. All but the F170W and F336W images were taken with the nucleus centered on the PC chip. For each filter, we combined the available images to create a cosmic ray free image without saturated pixels. The total counts from the nucleus in each filter were calculated by summing the counts out to a radius $4''.55$ after subtracting the background counts, which were determined using an annulus with radii between $4''.55$ and $6''.83$. It was necessary to use an aperture at least $4''$ in radius due to the broad wings on the HST point spread function (Holtzman et al. 1995). These counts were converted to the fluxes presented in Table 1 using the algorithms presented by Voit et al. (1997) and Whitmore, Heyer, & Baggett (1996). The uncertainties were assumed to be 15% for F160BW, F170W, and F1042M images. All other images were assumed to have an uncertainty of 10%. These values reflect the uncertainties in both the absolute calibration and determination of the background level.

Table 1. Photometric Observations

Filter	$\lambda_{\text{eff}}^{\text{a}}$ [Å]	$\Delta\lambda_{\text{eq}}^{\text{b}}$ [Å]	F_{λ} [10^{-15} ergs cm^{-2} s^{-1} Å $^{-1}$]	References
UIT-B1	1534	355	4.88 ± 0.73	1
F160BW	1554	575	6.33 ± 0.95	2
F170W	1695	520	6.03 ± 0.90	2
UIT-A1	2607	1147	2.34 ± 0.35	1
F300W	3045	879	5.12 ± 0.51	2
F336W	3349	495	5.36 ± 0.54	2
U	3641	641	4.41 ± 0.44	1
B	4421	960	9.31 ± 0.93	1
B	4421	960	9.39 ± 0.66	3
F555W	5314	1578	10.0 ± 1.00	2
V	5507	984	8.87 ± 0.89	1
R	6563	1591	10.3 ± 1.03	3
F814W	8365	2504	7.86 ± 0.79	2
F1042M	10444	854	7.01 ± 1.05	2
J	12302	2036	5.89 ± 0.59	2
H	16379	2863	3.80 ± 0.38	2
K'	21201	2882	1.86 ± 0.19	2

^a λ_{eff} was calculated by using the Set A PEGASE best fit model SED (see § 4)

^b $\Delta\lambda_{\text{eq}}$ was calculated by using eq. 5 of Gordon, Witt, & Friedmann (1998)

References. — (1) Massey et al. 1996; (2) this work; (3) Kormendy & McClure 1993

Table 2. WFPC2 Images

Image Name	Filter	Exp. Time [sec]
U3MR0101M	F160BW	1200
U3MR0102M	F160BW	1200
U2YE0207T	F170W	900
U2YE0209T	F170W	900
U3MR0103M	F300W	800
U3MR0104M	F300W	800
U2YE020BT	F336W	900
U2YE020DT	F336W	900
U2E20507T	F555W	400
U2E20508T	F555W	400
U2E20509T	F555W	400
U2E2050AT	F555W	400
U2E2050BT	F555W	40
U2E2050CT	F555W	40
U2E2050DT	F814W	400
U2E2050ET	F814W	400
U2E2050FT	F814W	400
U2E2050GT	F814W	40
U2E2050HT	F814W	40
U2E20501T	F1042M	500
U2E20502T	F1042M	500
U2E20503T	F1042M	700
U2E20504T	F1042M	300
U2E20505T	F1042M	500
U2E20506T	F1042M	500

Near infrared images at J , H , and K' of the central region of M33 were taken on 1998 March 2 (UT) using the NSFCAM instrument on NASA's Infrared Telescope Facility (IRTF). The detector was a 256×256 InSb array with an image scale of $0''.3/\text{pixel}$ giving a field-of-view of $76''.3$. For each filter, four images were taken alternating with four sky exposures. The sky images were combined using a sigma clipping algorithm giving a final sky image without stars. The flatfield image was calculated by subtracting a dark image from the sky image and normalizing the result. Each of the images of M33 was sky subtracted and flat fielded before being combined using the sigma clipping algorithm to remove cosmic rays and bad pixels. The calibration of the images was done using standard stars from Hunt et al. (1998) chosen to bracket ($J - K$) colors between -0.15 and 0.63. The standard stars were observed throughout the night bracketing airmasses between 1.0 and 2.2. The K magnitudes by Hunt et al. (1998) were converted to K' magnitudes using $K' = K + 0.2(H - K)$ (Wainscoat & Cowie 1992). Total exposure times were 80 seconds for each of the three filters. The J , H , and K' magnitudes of the nucleus were extracted using a sky annulus with radii between 40 and 60 pixels. The magnitudes were transformed from the CIT system to the homogeneous system defined by Bessell & Brett (1988). The zero points for the J , H , and K' magnitudes were taken from Bessell et al. (1998) and the resulting fluxes are given in Table 1. These fluxes are consistent with those given by Gallagher et al. (1982) within the uncertainties.

2.2. Spectroscopy

International Ultraviolet Explorer (IUE) observations provide the only ultraviolet spectra of the M33 nucleus. The observations used the large aperture ($10'' \times 20''$). Examining the line-by-line (SILO) spectra of the two IUE observations with similar position angles (SWP 52142 and LWP 1584), we found two sources were present. Using the MGEX and NEWCALIB routines provided in the IUEIDL package (Nichols et al. 1994), we extracted and calibrated the two spectra. We imposed the IUE aperture on the UIT images of M33 and confirmed that one of the spectra was from the nucleus and one was from a nearby star (UIT 219, $d = 10''$, Massey et al. 1996). The integrated flux from the UIT images (FUV0496 and NUV0402) in the IUE aperture matched that of the sum of the two spectra within the uncertainties.

Optical spectroscopy of the M33 nucleus was obtained using the GoldCam CCD spectrometer on the 2.1-meter telescope at Kitt Peak National Observatory on 1998 June 29 (UT). Grating #201 was used with a slit width of $240 \mu\text{m}$ ($3''$) resulting in a resolution of 19 \AA FWHM over a spectral range from 3300–9100 \AA . In the spatial direction, the slit extended $5'.2$ with a scale of $0.78'' \text{ pix}^{-1}$. The M33 spectrum was obtained in a single 900 sec exposure with a position angle of 100° and at an airmass of 1.39. The flat field used in reducing this spectrum was constructed from exposures of a quartz lamp corrected for the slit illumination function using twilight sky exposures. The spectrum was wavelength calibrated using HeNeAr lamp exposures taken throughout the night. The rms deviation of the adopted solution about the comparison line wavelengths was $\leq 1.0 \text{ \AA}$. Atmospheric H_2O and O_2 bands were removed using observations of

hot stars and the method described by Bica & Alloin (1987). A mean sky frame was constructed from several exposures of galaxies that did not fill the spatial direction on the chip. This frame was subsequently scaled to match the night sky lines in the M33 spectrum and subtracted from the M33 image. A 1-dimensional spectrum was extracted using a $10''$ aperture centered on the M33 nuclear spectrum. The non-nuclear contribution to the spectrum was subtracted by fitting a 5th degree polynomial to the galactic background along the spatial direction. The resulting spectrum was flux calibrated using several observations of spectrophotometric standards and the mean extinction coefficients appropriate for KPNO.

The optical spectrum of the M33 nucleus is shown in Figure 1 with the strong lines identified (Bica & Alloin 1986, 1987). Our spectrum is similar to that given in Figure 1 of Schmidt et al. (1990) except ours has a slightly steeper slope and a more pronounced Paschen jump. In addition, our spectrum is absolutely calibrated while the Schmidt et al. (1990) spectrum was only relatively calibrated.

The near-IR observations were made using the Steward Observatory infrared spectrometer, FSpec (Williams et al. 1993), on the Multiple Mirror Telescope (MMT) on 1996 June 21, 22 (UT). The spectra were taken using the medium resolution, 300 lines/mm grating. Four wavelength settings were used, *J*-band from 1.15 to 1.35 μm , *H*-band from 1.54 to 1.77 μm and two settings at *K*-band, from 2.015 to 2.23 μm and from 2.19 to 2.41 μm . The spectral resolution, as measured via OH sky emission lines, or Neon Krypton calibration lamps in the case of the long wavelength *K*-band, corresponded to approximately 2.5 resolution pixels (21 Å), or $R \approx 590$ at 1.25 μm , $R \approx 780$ at 1.65 μm , $R \approx 1000$ at 2.12 μm and $R \approx 1100$ at 2.3 μm . The same observing procedure was used on both nights and with all grating positions. The spectrometer has a slit size of $1.2'' \times 32''$ on the MMT. This allowed for four unique positions as the M33 nucleus was stepped $\approx 6''$ along the slit. The integration time at each position was 2 minutes giving a total of 8 minutes per set of observations. A total integration of 24 minutes was obtained at both *J*- and *H*-band. At 2.12 μm (short *K*-band) and 2.30 μm (long *K*-band), the total integration times were 40 and 32 minutes respectively.

The reductions made use of a dark-current-corrected flat field obtained from a uniformly illuminated screen. After dark current had been subtracted and the flat field divided into the raw two-dimensional images, sky emission (and additional thermal background in the *K*-band) was removed by subtracting one slit position from the next. In many cases, a few percent scaling was required to get the telluric atmospheric OH features to disappear entirely. Background renormalization by a few percent was also required to remove fluctuations in thermal background between integrations in the *K*-band. Interspersed between our M33 observations, we obtained spectra at a similar airmass of HR 410, a late F dwarf, to be used to remove telluric artifacts. Intrinsic features in the spectrum of this star were removed using a Kurucz model atmosphere, with $T_e = 6500$, $\log(g) = 4.5$, solar abundance. Dividing the spectrum of M33 by this modified stellar spectrum allowed us to cancel features due to the atmosphere. While our near-infrared spectra are not flux calibrated (due to slit loss and non-photometric conditions) we can determine

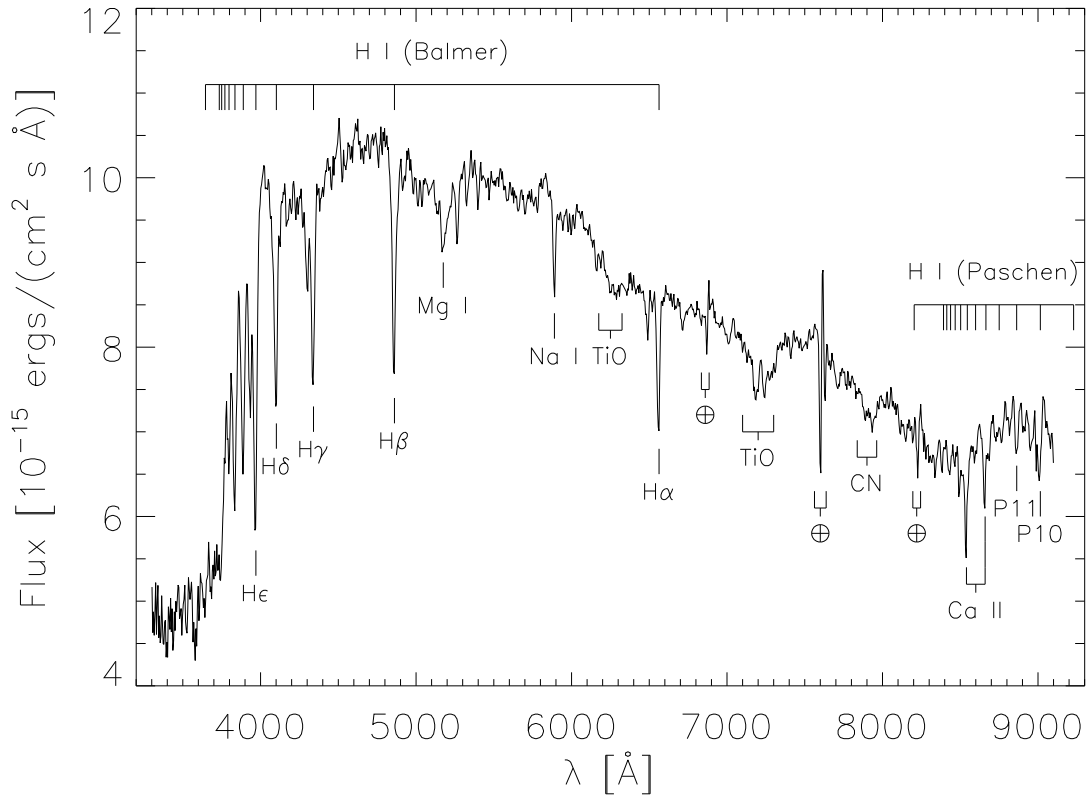


Fig. 1.— The optical spectrum of the M33 nucleus is plotted along with identifications of the strong lines. The telluric identifications (\oplus) refer to residuals left over from the removal of the atmospheric H₂O and O₂ bands.

the accurate relative flux distributions for each grating position.

The long slit of FSpec allowed us to look for evidence of light extended beyond the nuclear region. While there likely is some low level flux outside the nucleus, dividing one slit position by another in the reductions revealed no structure outside of the nuclear point source. Measurement of the full-width, half-maximum flux of the nucleus along the slit also reveals the nucleus to be unresolved spatially. Typical seeing during the observations was very good, approximately 1 to 1.5"; however by the end of the integration, the multiple mirrors of the MMT drifted slightly relative to each other on the sky, reducing the effective seeing to $\sim 2''$.

3. The Starburst Model

To model the spectral energy distribution (SED) of a starburst region, we need to model the stellar and gas emission accurately, including the modification of this emission by absorption and scattering by dust in the starburst region. Other input parameters include the distance to the starburst, the radial velocity of the starburst, and the dust column in our Galaxy towards the starburst. For the M33 nucleus, the distance is 795 kpc, the foreground dust column has an $E(B - V) = 0.07$ and was assumed to be Milky Way (MW) dust with $R_V = 3.1$ (Cardelli, Clayton, & Mathis 1989), and the radial velocity is -172 km s^{-1} (Zaritsky, Elston, & Hill 1989; van den Bergh 1991).

The starburst model is an improved version of that used by Gordon et al. (1997). The stars and gas in a starburst are modeled using Leitherer et al. (1995, 1998; hereafter L98) and Floc & Rocca-Volmerage (1997, 1998; hereafter PEGASE) stellar evolutionary synthesis (SES) models. We used two SES models in an attempt to estimate the uncertainties in the model SEDs due to uncertainties in the assumed stellar evolutionary tracks, stellar spectra, and computational algorithms. Both models were run for burst and constant star formation scenarios, an initial mass function (IMF) with a Salpeter (1955) slope ($\alpha = 2.35$), a mass range of 0.1–100 M_\odot , and solar metallicity. The L98 model used Geneva evolutionary tracks and the PEGASE model used Padova evolutionary tracks.

The choice of a Salpeter IMF for stellar masses greater than $\sim 0.85 M_\odot$ is supported by the observations in Local Group clusters and associations (Hunter et al. 1997). Furthermore, IMF8, found by Rieke et al. (1993) to be optimum for the M82 starburst, has a net high mass slope similar to the Salpeter value. There are no direct constraints on the form of the IMF below $0.85 M_\odot$ in starburst-type regions, but the local IMF has a slope of $\alpha \sim 1$ below masses of $\sim 0.7 M_\odot$ (e.g., Scalo 1998). For this work, we assume the IMF has the form

$$N(m) = Cm^{-\alpha} = \begin{cases} Cm^{-2.35} & m > 0.7 M_\odot \\ 1.619Cm^{-1} & m < 0.7 M_\odot \end{cases} \quad (1)$$

where C is the normalization constant of the IMF. The use of a different IMF below $0.85 M_\odot$ changes the total mass needed for the burst, but does not affect the computed SED for the ages

Table 3. Near-Infrared Line Identifications and Equivalent Widths

Ion	Transition	Vacuum λ [μm]	Equiv. Width [\AA]
J band			
??		1.196	1.5
H I	(3-5)	1.2818	1.5
H band			
¹² CO	(3,0)	1.558	1.3
??		1.565	0.8
Mg I	(4s-4p, tr)	1.577, 1.575, 1.575	$\sim 3.0^{\text{a}}$
¹² CO	(4,1)	1.578	"
Si I		1.5894	2.5
Si I	(4p-5s)	1.596	0.3
¹² CO	(5,2)	1.598	1.5
H I	(4-13)	1.6109	≤ 1
¹² CO	(6,3)	1.619	2.5
H I	(4-12)	1.6407	1.8
??		1.6525	1.3
¹² CO	(8,5)	1.662	4.0
H I	(4-11)	1.6811	< 1
Mg I	(4s-4p)	1.7146	4.6
¹² CO	(10,7)	1.7067	2.0
Fe I		1.7307	1.2
Si I		1.7332	2.0^{a}
H I	(4-10)	1.7362	"
K band			
??		2.0443	1.0
Fe I		2.0704	~ 1
Si I	(4p-5s)	2.1360	≤ 1
H I	(4-7)	2.1661	2.0
Ti I		2.1789	~ 0.3
Si I		2.1885	1.0
Na I		2.2062	~ 1
Na I		2.2090	< 0.5
¹² CO	(2,0)	2.2935	~ 10
¹² CO	(3,1)	2.3227	~ 8
¹³ CO	(2,0)	2.3448	~ 3.5
¹² CO	(4,2)	2.3525	~ 9
¹³ CO	(3,1)	2.3739	~ 4
¹² CO	(5,3)	2.3830	~ 5.5
¹³ CO	(4,2)	2.4037	~ 2.5

^aBlended

appropriate for the M33 nucleus. For example, using the IMF given in equation 1 would imply 59% of the mass given by the assumption of a Salpeter slope for the entire IMF. To obtain realistic masses, we have therefore multiplied the model values by 0.59.

The metallicity of the M33 nucleus should be similar to the surrounding region and the central abundances of M33 are approximately solar (Garnett et al. 1997; Monteverde et al. 1997). SEDs were produced for ages up to 1×10^9 years for L98 and 1.9×10^{10} years for PEGASE. Both models used the Lejeune, Cuisinier, & Buser (1997) spectral library which has a resolution of $\sim 40 \text{ \AA}$. An additional input to both models is the fraction of Lyman continuum photons which contribute to the nebular emission (the rest are assumed to be absorbed by dust). Since the nucleus of M33 does not show any emission at $H\alpha$, the contribution to the SED from nebular emission is negligible and the value of this model parameter is unimportant.

Both SES models produce similar SEDs for ages between 10 and 100 million years (Myrs). For ages < 10 Myrs, there are quite significant differences in the optical/IR between the SEDs which can be traced to the different evolutionary tracks used (Geneva versus Padova; Fioc & Rocca-Volmerange 1997). After 100 Myrs, the PEGASE model produces consistently higher IR fluxes, which is due to the inclusion of the thermally pulsating asymptotic giant branch (TP-AGB) evolutionary tracks in this model (Fioc & Rocca-Volmerange 1997). These tracks are not included in the L98 model, limiting its validity to ages < 100 Myrs (C. Leitherer 1998, private communication).

The effects of dust were modeled using a Monte Carlo radiative transfer code (Witt 1977; Witt & Gordon 1996; Gordon et al. 1997; Witt & Gordon 1998). Calculation of the radiative transfer through dust is crucial when any geometry other than the screen geometry is suspected. Our radiative transfer model was run for dust global geometries characterized as dusty (dust, stars, and gas uniformly mixed together) and shell (a sphere of stars and gas enshrouded by a shell of dust). These two geometries define the extremes one would expect for star formation regions. The local dust geometry was characterized with inter-clump to clump density (k_2/k_1) ratios between 1.0 and 0.001 and a clump filling factor of 15%. In a given model, the physical properties of the dust grains (τ_λ , albedo, and scattering phase function) were characterized by either MW ($R_V = 3.1$, Cardelli, Clayton, & Mathis 1989) or Small Magellanic Cloud Bar (Gordon & Clayton 1998) type dust (Gordon et al. 1997). The amount of dust is parameterized by the V band optical depth, τ_V . The dust models were run for τ_V values ranging from 0.25 to 50.

Combining the SES and dust radiative transfer models provides a model for the SEDs of starburst regions which accurately includes stars, gas, *and* dust. The parameter space covered by the starburst model is large and, as a result, an algorithm to determine which of the model SEDs fit the observed SED was needed. Following Gordon et al. (1997), we use the $\tilde{\chi}^2$ (reduced χ^2) method. The $\tilde{\chi}^2$ was computed using

$$\tilde{\chi}^2 = \frac{1}{d} \sum_{i=1}^n \left[\frac{F_o(\lambda_i) - F_m(\lambda_i)}{\sigma(\lambda_i)} \right]^2 \quad (2)$$

where n is the number of points in the observed SED, d is the number of degrees of freedom, $F_o(\lambda_i)$ is the observed flux at the i th point in the SED, $F_m(\lambda_i)$ is the same for the model flux, and $\sigma(\lambda_i)$ is the i th uncertainty in the observed flux (Taylor 1982). In the paper by Gordon et al. (1997), a typographical error resulted in the square being left off the term in the sum of Equation 2. In an attempt to also account for the observational uncertainties in the SES and radiative transfer model predictions, we have added, in quadrature, a 15% (10%) uncertainty to $\sigma(\lambda_i)$ of the ultraviolet/infrared (optical) observations. The uncertainties associated with the SES models are due to their use of observational spectra to calibrate the stellar SEDs (Lejeune et al. (1997)). The uncertainties associated with the radiative transfer model are due to the use of observationally determined values of the physical properties of dust grains. The 10-15% uncertainty quoted above for the starburst model is a reasonable assessment of these uncertainties. In fitting the model SEDs to the observed SED, there are 4 parameters which are derived from the observed SED (age, mass, τ_V , and k_2/k_1). Thus, $d = 17 - 4 = 13$. In our fitting algorithm, all of the model SEDs were computed for the input distance, reddened by the foreground dust, and then shifted to the rest frame of M33.

4. Model Fits

The model SEDs were fitted to the photometric data given in Table 1. The model fluxes in the observed photometric bands, $F_m(\lambda_i)$, were calculated by convolving the band transmission curves (Bessell & Brett 1988; Bessell 1990; Biretta et al. 1996; Stecher et al. 1997; M. Bessell 1998, private communication) with the full resolution model SEDs. We examined all model SEDs which had $\tilde{\chi}^2 < 2.14$ as this includes all model SEDs which fit with a $>1\%$ significance, i.e. the probability of the correct model getting a higher $\tilde{\chi}^2$ [$P_{13}(\tilde{\chi}^2 \geq 2.14)$] is only 1%. These model SEDs were grouped into two sets, (A) those with ~ 70 Myr old burst of star formation and (B) those with ~ 1 Gyr of constant star formation. For both sets, no models with a dusty geometry fit the observations. The best fit model parameters for set A and B are given in Table 4. The uncertainties on these parameters were determined by the 99% confidence level as described above. The observed photometric SED of the M33 nucleus is plotted in Figure 2 along with the best fit model SEDs in from both Set A and B. The Set A models fit the photometric SED better than the Set B models according to the $\tilde{\chi}^2$ values (Table 4). This can be seen in Figure 2 where the best fit Set B model SED is consistently too high in the far-UV, too low in the optical, and too high in the IR.

The validity of Sets A and B can be tested further with the spectroscopic observations. The UV, optical, and IR spectra of the M33 nucleus are plotted in Figures 3-5. As the spectroscopic data were taken with different apertures, it is not possible to fit simultaneously the UV to near-IR spectroscopy of the M33 nucleus. In addition, the use of relatively large apertures results in the flux from the nucleus being diluted by flux from the surrounding region. Therefore, we have used the photometric data along with the spectra for the comparisons with the best fit model SEDs.

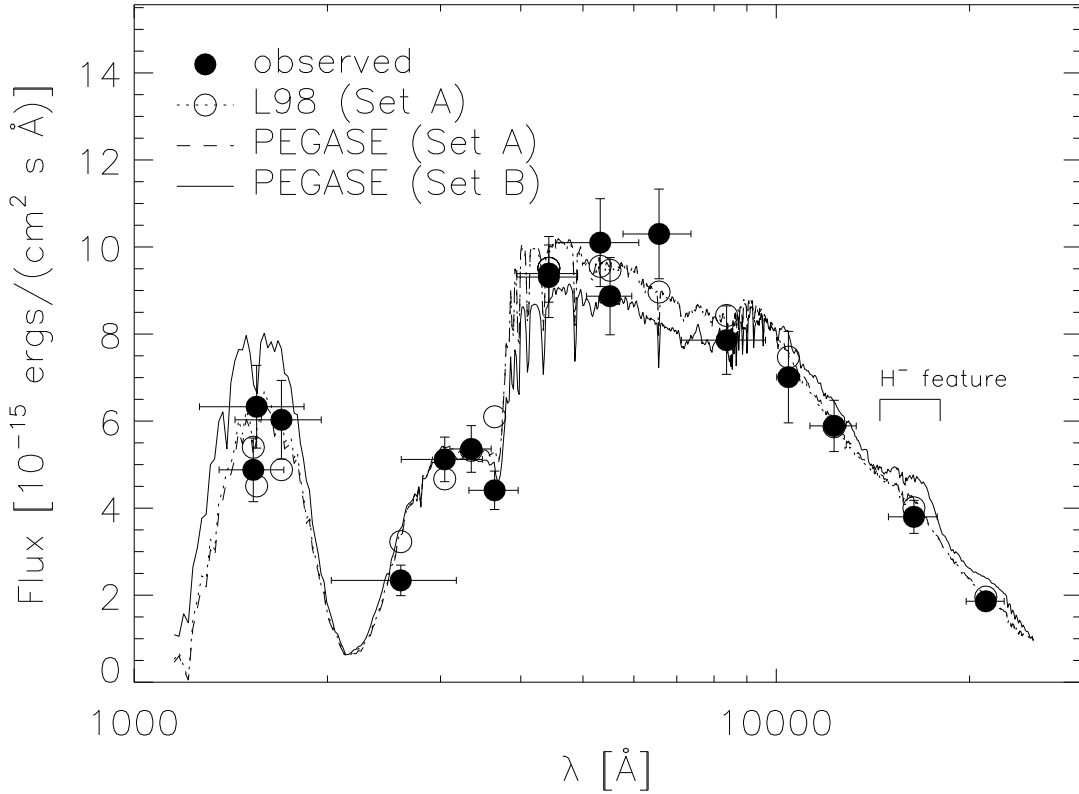


Fig. 2.— The observed photometric SED and best fit model SEDs for both Set A and B are plotted. The horizontal error bars on the observed SED points represent the bandwidth of the observations. The open circles give the fluxes in the bands corresponding to the observed photometry. They were determined using the band response curves and the L98 best fit model SED. The $1.6 \mu\text{m}$ H^- feature is identified (see §4).

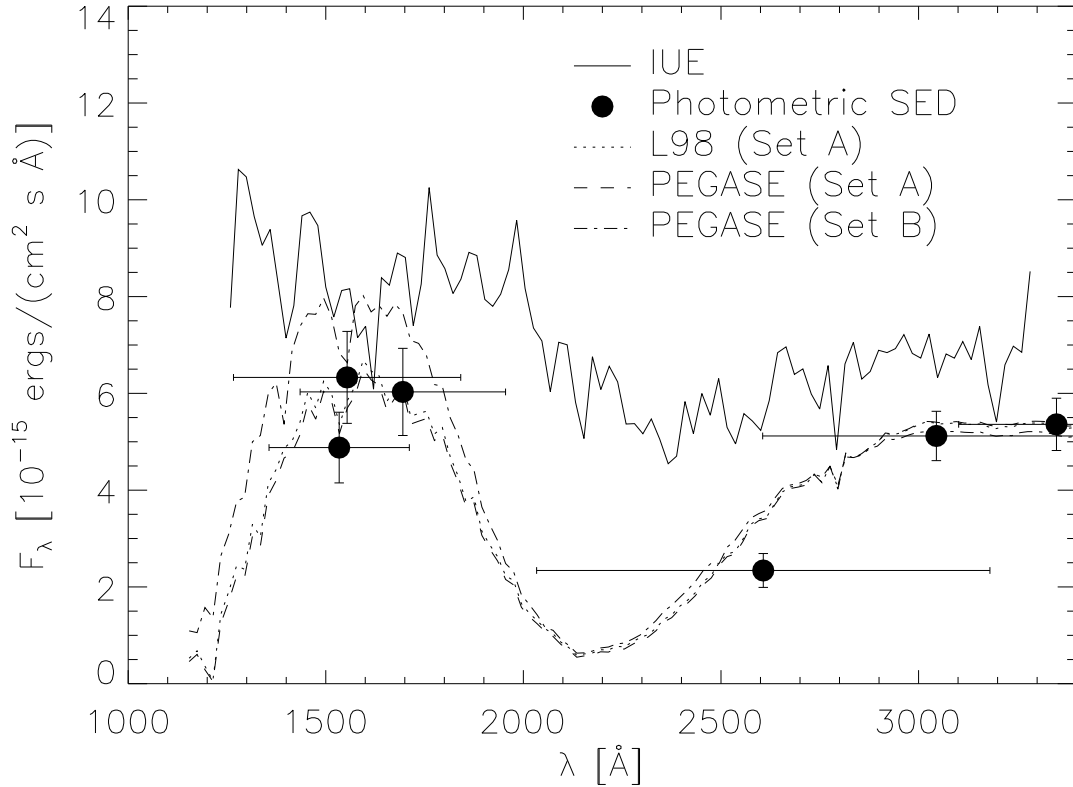


Fig. 3.— The IUE spectrum of the M33 nucleus and surrounding region is plotted. In addition, the photometric SED and best fit model SEDs for Sets A and B are plotted.

Figure 3 plots the IUE spectrum along with the photometric SED and the best fit model SEDs from Sets A and B. Due to the faintness of the M33 nucleus, the S/N in the IUE spectrum is quite low. We display the spectrum with 20 Å bins to increase the S/N and match the resolution of the model SED. The IUE spectrum obviously includes flux from both the nucleus and the surrounding region since the photometric SED is always below the IUE spectrum. The shape of the IUE spectrum is flatter than the photometric and model SEDs, implying that the UV spectrum of the region surrounding the nucleus has a much smaller depression at 2175 Å and, therefore, is attenuated by less dust than the nucleus. This behavior arises from mixing flux from regions which have differing amounts of dust: the least attenuated region will contribute disproportionately to the flux, washing out the signatures of dust.

The optical spectrum of the M33 nucleus is plotted in Figure 4 along with the best fit model SEDs from Sets A and B. Unlike the IUE spectrum, the optical spectrum is roughly consistent with the photometric SED. While the steeper slope makes the observed spectrum slightly bluer

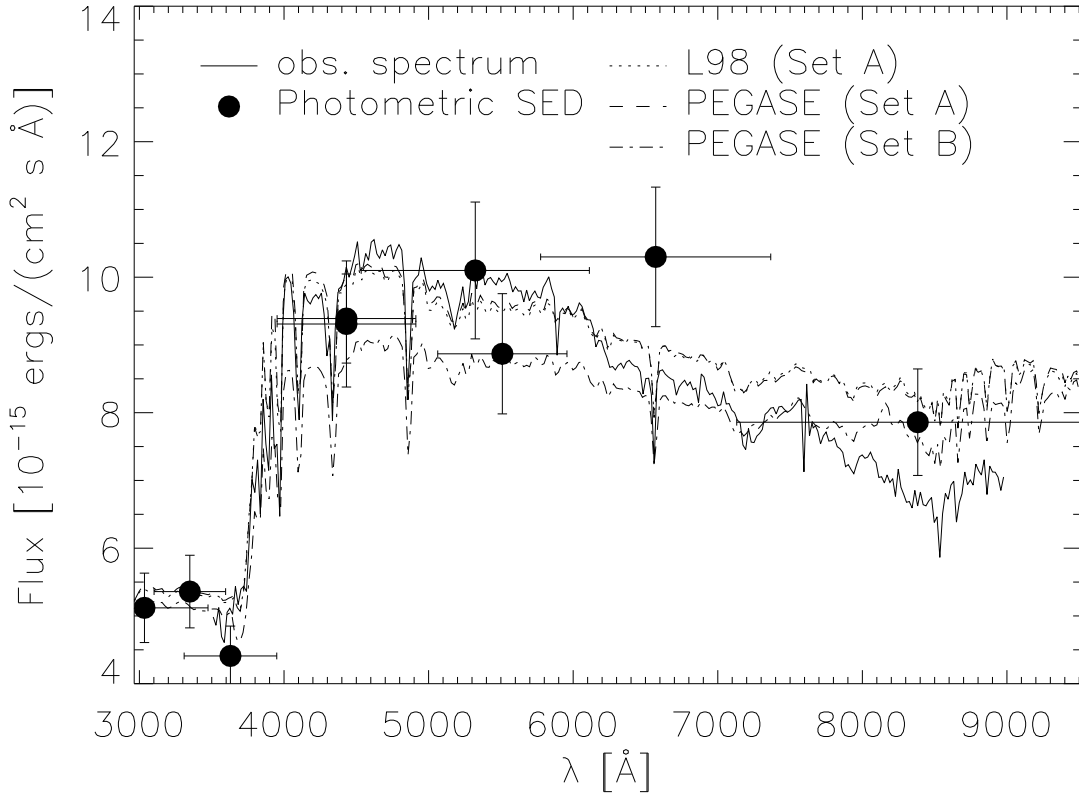


Fig. 4.— The optical spectrum is plotted along with the best fit model SEDs from Set A and B. The optical spectrum has been rebinned to match the resolution of the model SEDs.

than all of the model SEDs, the strengths of the features are comparable, with some notable exceptions. For example, the observed strength of the Na I $\lambda 5889$ (1.8 \AA) can be traced to the presence of a large amount of interstellar material. This is consistent with our detection of a shell of dust with $\tau_V \sim 2$ enshrouding the nucleus. Both the differing line strengths and the bluer color could arise from inclusion of flux from the region surrounding the nucleus as the observed spectrum includes light from a $3'' \times 10''$ region. The general agreement with the nuclear photometric levels would still be consistent if some of the nuclear flux spilled out of the slit (the seeing was $\sim 2''$).

The optical spectrum shows no significant emission in $H\alpha$ or any other line. Set B models predict $H\alpha$ in emission with an equivalent width of $\sim 100 \text{ \AA}$ which would easily have been seen in the observed spectrum. The SES models predict the strength of $H\alpha$, but do not add them to their output SEDs. Thus, no emission lines are seen in Figure 4 for the Set B model SED even through they would be very prominent. In comparison, the Set A models predict no detectable $H\alpha$ emission, in good agreement with the observations.

The infrared spectra are plotted in Figure 5. All the models do a fairly good job of fitting them, as expected since all the model SEDs fit the photometric SED. Most of the observed absorption lines are present in the model SEDs, but not necessarily at the same strength. The model SEDs have much weaker Brackett lines than observed (H I (4-12) and H I (4-7) are good examples, but we also detect H I (4-10)), and they do not show the ^{13}CO lines. Furthermore, the ^{12}CO bands are somewhat weak in the models, both at the first overtone near $2.3\ \mu\text{m}$ and the second near $1.6\ \mu\text{m}$. Since the inputs to the infrared models have greater uncertainty and are less complete than those for the optical, it is not surprising that this is also the region where the models are most deviant.

There is only one infrared spectral feature that differs significantly between the Set A and B models, the broad $1.6\ \mu\text{m}$ H^- peak is seen in stars with $T_{\text{eff}} < 6000\text{K}$ (Lançon & Rocca-Volmerange). This feature is not seen in the observations (Figure 2 and 5b), which suggests that the Set A models better describe the M33 nucleus than the Set B models. The Set B models reproduce the slope of the observed short K band spectrum (Figure 5c), but given the difficulties in determining general slopes in the data, this disagreement is probably not significant.

Because of its sensitivity to the stellar luminosity, the CO band strength has proven useful in determining the age of starbursts. This parameter is commonly expressed as a "CO index" based on the average depth of the feature in intermediate width photometric bands (Frogel et al. 1978). We have used the formulation of Doyon, Joseph, & Wright (1994) to compute CO indices for our observations of M33 and for the L98 and PEGASE synthetic spectra. For M33, the index is approximately 0.21. The synthetic spectra show obvious shortcomings in both cases, such as discontinuous changes in index strength for the PEGASE models and an index that never reaches the highest observed strengths for L98. For the starburst models of Rieke et al. 1993, the CO index of the individual stellar types was carefully calibrated empirically against the extensive available photometric observations. The run of CO index with starburst age for these models (Shier, Rieke, & Rieke 1996) does not have the problems we find in the synthetic spectra, and we prefer it for comparison with M33. There are two cases that represent a relatively short burst, either a star formation rate Gaussian in time with a full width at half maximum of 5 Myr, or a burst that starts abruptly and decays with an exponential time constant of 20 Myr. These cases produce an index of 0.21 after 50 to 70 Myr, in excellent agreement with the parameters of the burst we have derived from the spectral synthesis in the optical and ultraviolet.

5. Discussion

5.1. Nuclear Mass

Assuming the rotation curve of M33 is flat within $4''$, Kormendy & McClure (1993) calculate an upper limit of $2.1 \times 10^6 M_{\odot}$ on the mass of the nucleus. Lauer et al. (1998) calculate a lower limit by determining a core mass of $2 \times 10^4 M_{\odot}$. A better estimate of the mass in the starburst

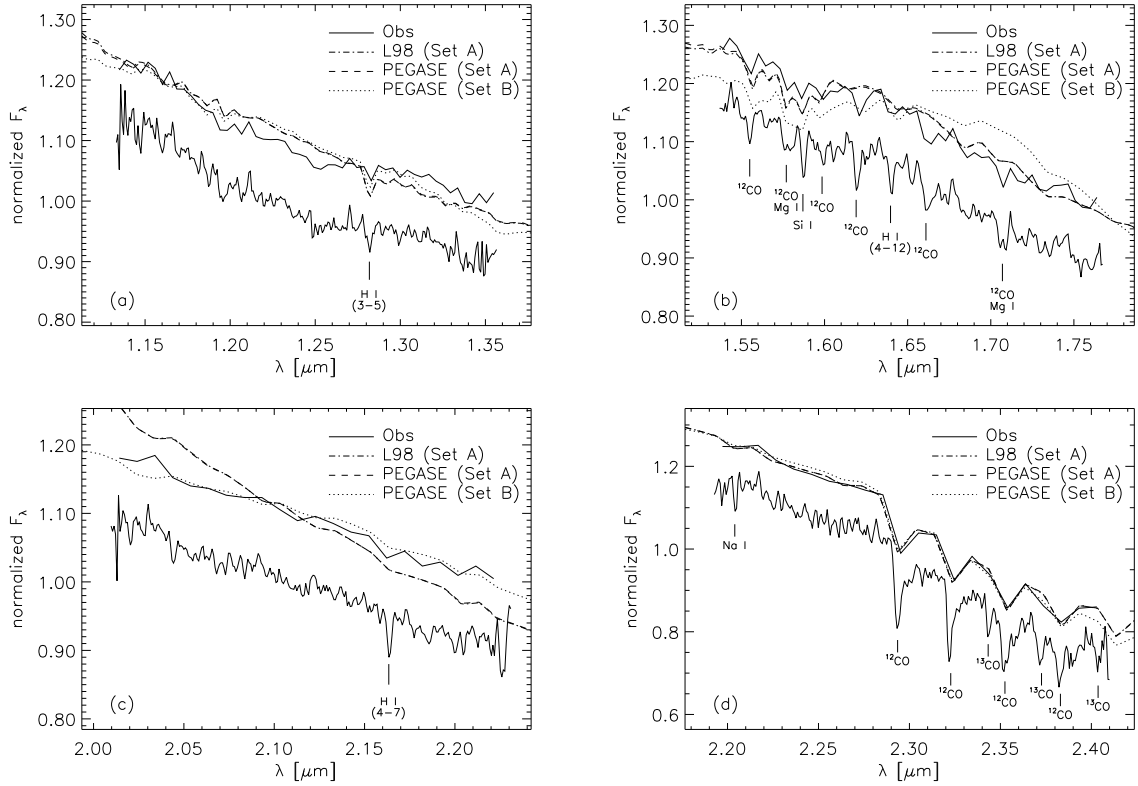


Fig. 5.— The observed IR spectra are plotted along with the best fit model SEDs. The J band spectrum is plotted in (a), the H band in (b), and the two K band spectra in (c) and (d). As the observed spectra are only relatively calibrated, the model SEDs are plotted normalized to the average value of the observed spectrum. The lower observed spectrum is plotted at the observed resolution and the upper observed spectrum is plotted at the model resolution (100 Å for J & H band, 200 Å for the K band).

region should be possible from the measured velocity dispersion (21 km s^{-1} , Kormendy & McClure 1990) and the size of the starburst.

We measured the FWHM of the PC images of the M33 nucleus by fitting them with 2-dimensional Gaussian convolved with the TinyTim point spread function (PSF) appropriate for each filter (Krist & Hook 1997). It was not possible to fit the nucleus in the F160BW filter due to its low signal. The results are given in Table 5. Lauer et al. (1998) found the FWHM was $0''.07$ (0.27 pc) in the F555W image using a different analytic form for the nuclear profile and taking better care to correct for the effects of the PSF and aliasing. The increasing size of the nucleus as a function of wavelength confirms the color gradient measured by Kormendy & McClure (1993) and Lauer et al. (1998).

Because they dominate the light, the observed velocity dispersion and size reflect only properties of the more massive stars. This is confirmed by the composite spectral type of the nucleus, for which a range from late-A to early-F main sequence has been reported (Morgan & Mayall 1957; van den Bergh 1991; Massey et al. 1996; B. Garrison, private communication). Assuming equipartition in kinetic energies, the true velocity dispersion (σ_t) of the nucleus is then

$$\sigma_t = \sigma_o \left(\frac{m_o}{m_t} \right)^{1/2} \quad (3)$$

where σ_o is the observed velocity dispersion, m_t is the average mass of the stars in the nucleus, and m_o is the average mass of the stars contributing to σ_o . Assuming the IMF given in equation 1, $m_t = 0.84 M_\odot$. From the spectral type of the nucleus, $m_o \approx 3 M_\odot$. Thus, the true velocity dispersion of the nucleus is 40 km s^{-1} . The virial mass is computed from

$$M_{VT} = \frac{3R\sigma_t^2}{G} = 698R\sigma_t^2 \quad (4)$$

where R is the effective radius of the nucleus in pc, σ_t is in km s^{-1} , and M_{VT} is in M_\odot . Estimating R for the nucleus is nontrivial and so we will use a measured R value and compute a lower limit. We assume R to be the size of the nucleus as measured in the F814W image (HWHM = $R = 0.41 \text{ pc}$) since σ_o was measured from the Ca II infrared triplet (Kormendy & McClure 1993). The mass of the nucleus is then $> 4.6 \times 10^5 M_\odot$. This is similar to the $6 - 7 \times 10^5 M_\odot$ of the best fit Set A models.

In addition to the starburst population, it is likely there is at least one other stellar population in the nuclear region. The presence of an older ($\sim 1 \text{ Gyr}$) underlying stellar population with a large M/L_V is strongly implied by the growth of surface brightness and stellar counts approaching the nuclear region (Minniti, Olszewski, & Rieke 1993) and the mass ($2.1 \times 10^6 M_\odot$) of the inner $4''$ of M33 (Kormendy & McClure 1993). Within $4''$, $3/4$ of the observed V band flux comes from the nucleus (Kormendy & McClure 1993). This implies that the other stellar population in the nuclear region has a M/L_V ratio of 5.5 assuming the Set A best fits or 1.8 assuming the Set B best fit. Thus, the mass required by the Set A models ($6 - 7 \times 10^5 M_\odot$) is more consistent with the available data on the nuclear region.

Table 4. Best Fit Model Parameters^a

parameter	L98	PEGASE	
	Set A	Set A	Set B
star formation type	burst	burst	constant
geometry	shell	shell	shell
dust type	Milky Way	Milky Way	Milky Way
age [years]	$65_{-30}^{+30} \times 10^6$	$70_{-30}^{+110} \times 10^6$	$1_{-0.2}^{+0.2} \times 10^9$
mass [M_{\odot}]	$6.4_{-2.7}^{+3.7} \times 10^5$	$6.9_{-2.2}^{+2.3} \times 10^5$	$1.2_{-0.1}^{+0.2} \times 10^6$
k_2/k_1	$0.5_{-0.45}^{+0.5}$	$0.5_{-0.45}^{+0.5}$	$1.0_{-0.5}^{+0}$
τ_V	$2_{-0.25}^{+1.25}$	$2.13_{-0.75}^{+0.75}$	$2_{-0}^{+0.12}$
$\tau_{V,\text{eff}}$	$1.26_{-0.18}^{+0.36}$	$1.33_{-0.5}^{+0.27}$	$1.26_{-0}^{+0.08}$
M/L_V [$M_{\odot}/L_{V,\odot}$]	$0.13_{-0.06}^{+0.03}$	$0.12_{-0.05}^{+0.1}$	$0.22_{-0.03}^{+0.03}$
$\tilde{\chi}^2$	1.39	1.44	1.96

^aThe uncertainties quoted are for the 99% confidence level ($\sim 3\sigma$).

Table 5. Nucleus Size

Filter	FWHM		
	[pixels]	[$''$]	[pc]
F300W	2.65	0.12	0.46
F555W	4.33	0.20	0.77
F814W	4.62	0.21	0.81
F1042M	5.58	0.25	0.98

5.2. Stellar Population

The photometric and spectroscopic evidence indicate that Set A models fit the observations of the M33 nucleus better than the Set B models, as does the mass determination. The Set A models are consistent with the small size of the nucleus and flat profile of the inner disk of M33. The flat profile implies there is a lack of a substantial density gradient which could funnel gas to the nucleus (Kormendy & McClure 1993), which means fueling continuous star formation (as Set B fits would require) would be difficult. The stellar population of the M33 nucleus is described by a 35 to 180 Myr burst of star formation with a mass of $0.4\text{--}1.1 \times 10^6 M_{\odot}$ (Table 4). The best fit SEDs in Set A for both SES models give very similar results. They imply the best description of the M33 nucleus is a burst of star formation 70–75 Myrs old and a mass of $\sim 0.7 \times 10^6 M_{\odot}$ (Table 4).

Our finding that the M33 nucleus is well described by a single burst of star formation enshrouded by a significant amount of dust is quite different than previous studies (O’Connell 1983; Ciani, D’Odorico, & Benvenuti 1984; Schmidt et al. 1990). In these studies, the role of dust was underestimated and, as a result, luminous young and old stellar populations were both needed to reproduce the relatively red (flat) spectrum of the M33 nucleus. For example, Ciani et al. (1984) modeled the IUE spectrum plus U , B , and V photometry of the M33 nucleus. They found that the data were best represented by two stellar populations, one extremely young ($\sim 10^7$ years) and one old ($\sim 10^{10}$ years). They argued that the effects of foreground and internal dust were well represented by a screen of MW-type dust with an $E(B - V) = 0.06$. Schmidt et al. (1990) obtained a long-slit optical spectrum of the M33 nucleus with a $3''.5$ slit and modeled it using a combination of star clusters of different ages. They found that the M33 nucleus was composed of 7 star clusters with ages ranging from 10^7 to $> 10^{10}$ years. This is similar to other studies where over 50% of the V band light was claimed to be from stars with ages $> 5 \times 10^9$ years. In addition, Schmidt et al. (1990) modeled the effects of dust as due to a Galactic foreground screen with $E(B - V)_G = 0.05$ and a M33 internal screen with $E(B - V)_i = 0.05$. The mass-to-light ratio (M/L_V) we compute from our model fits, corrected for foreground and internal dust, is ~ 0.1 . This is significantly different from previous studies, which found $M/L_V \sim 2\text{--}3$ (Gallagher, Goad, & Mould 1982; O’Connell 1983) which is in excess of the value likely to be present from dynamical considerations. By including dust properly, we have arrived at a simpler model of the M33 nucleus which reproduces its observed SED from the UV to the near-IR.

We can estimate the peak luminosity of the M33 starburst, although there is some uncertainty because our models do not constrain the rate of star formation with time uniquely. For example, the starburst mass in M33 is roughly 500 times less than that in M82, assuming similar IMFs (e.g., IMF8 of Rieke et al. 1993) and the somewhat extended burst which best fits the M82 data. Thus, at an age of ~ 10 million years, the M33 starburst would have luminosity of 0.002 times that of M82, or $\sim 10^8 L_{\odot}$. Alternately, from our abrupt burst model and the current luminosity of $1.4 \times 10^7 L_{\odot}$, the luminosity at 10 Myrs would have been $2.4 \times 10^8 L_{\odot}$. The center of the Milky Way contains a very compact ($r \sim 0.2$ pc) cluster of young (≤ 10 Myrs old) stars with

an integrated luminosity of $\sim 10^7 L_\odot$ (Rieke & Lebofsky 1982; Werner & Davidson 1989). The analogy between these two cases is striking. It appears that in M33 we may well be seeing a later development of an event virtually identical to the starburst that currently dominates the Galactic Center.

The relatively young age of the nucleus that we derive from our models may clear up another mystery. The M33 nucleus has a very strong X-ray source with a $L_X \sim 10^{39}$ ergs s $^{-1}$ (Trinchieri, Fabbiano, & Peres 1988; Schulman & Bergman 1995). The detection of a 106 day period requires that this object be a single source (Dubus et al. 1997). The only known type of object which could reproduce both observed effects is a stellar mass black hole ($\sim 10 M_\odot$) accreting from a companion star. This type of object was mentioned by Dubus et al. (1997), but discarded as the solution as previous work on the M33 nucleus argued against a significant population of O–B stars. The requirements of such an X-ray binary are a black hole with a companion star with enough mass to withstand the supernova blast that created the black hole without being ejected from the binary. For example, a black hole with an early B giant companion would be transferring a significant amount of matter to the black hole, resulting in the observed X-ray luminosity.

5.3. Nature of the Dust

The type, geometry, and amount of dust associated with the M33 nucleus is fairly well constrained by the observed photometric SED. The dust is best described by a shell of somewhat clumpy MW-like dust ($k_2/k_1 \sim 0.5$) with a radial V-band optical depth of ~ 2 . To show the effects of both foreground and internal dust on the intrinsic SED of the M33 nucleus, we present Figure 6. Even in the Galactic foreground dust corrected SED, the flux at 2607 Å (UIT-A1) is significantly lower than the flux in the bands around 1600 Å (UIT-B1, F160BW, and F170W) and around 3300 Å (F300W, F336W, U). The only known way to get such a depression in the SED of a stellar population is to attenuate its SED by dust with a 2175 Å feature, i.e. MW-type dust.

It is interesting to compare this with the result found by Gordon et al. (1997). They found that SMC-like dust was responsible for the attenuation in the 30 starburst galaxies in their sample. They used IUE-selected starburst galaxies, which biased their study towards intrinsically bright, lightly attenuated starburst regions. The interstellar environment near an intense starburst is very harsh, associated with an intense UV radiation density and supernovae shocks. There is evidence from the observed dust extinction curves in the Magellanic Clouds which suggests that star formation modifies nearby dust. In the SMC, the only extinction curve outside the star forming bar is very similar to that found in the Milky Way. The other three extinction curves in the bar are the most extreme known in terms of a non-existent 2175 Å bump and strong far-UV rise (Gordon & Clayton 1998). In the LMC, there are two different extinction curves (Misselt, Clayton, & Gordon 1998). The extinction curve associated with stars near the LMC 2 supergiant shell (which is itself near the 30 Dor star formation region) has a weak 2175 Å bump. The extinction curve associated with stars elsewhere in the LMC is similar to that found in the Milky

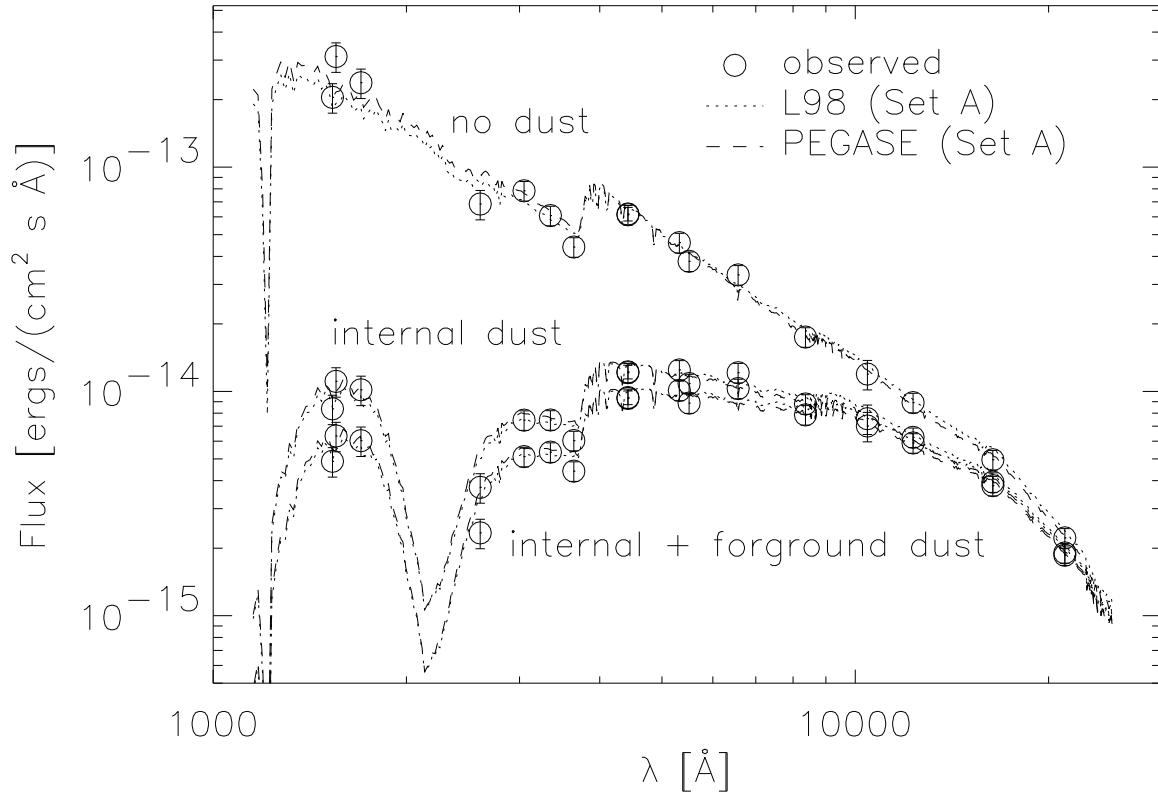


Fig. 6.— The photometric SED and two best fit model SEDs in Set A are plotted as observed (bottom), corrected for foreground Galactic dust ($\tau_V = 0.20$, middle), and corrected for both foreground and internal dust (top). The bottom set of open circles are the observed data. The middle and top set of open circles are what the observed data would look like corrected for foreground Galactic dust and for both internal and foreground dust.

Way. However, the 30 Dor region in the LMC exhibits much more intense star formation than any region in the SMC, but the most extreme extinction curves are found in the SMC. This fact implies that the relationship between star formation activity and the modification of nearby dust is not a simple one.

Recent theoretical models of dust exposed to shocks (Jones, Tielens, & Hollenbach 1996; O’Donnell & Mathis 1997) illustrate the complicated behavior expected for dust near active star formation. The number of small particles in shocked dust is increased through shattering of larger grains and results in an increased extinction in the far-UV. However, the models which produce a stronger far-UV rise, also produce normal or strong 2175 Å bumps. This is not what is seen in the behavior of dust in starburst galaxies or the Magellanic clouds and probably reflects our incomplete understanding of the carrier of the 2175 Å feature.

The M33 nucleus was also observed by IUE, but is not typical of the IUE sample used by Gordon et al. (1997). M33 is much closer than the majority of the IUE sample (0.795 versus 60 Mpc) and its faintness implies it is intrinsically fainter and/or suffers a higher attenuation than the rest of the sample. In the case of M33, the starburst is surrounded by a larger optical depth of dust and, since it lacks emission lines, is older than those seen in the IUE sample. Thus, the dust in the M33 nucleus has likely undergone less processing since it is near a small starburst and self-shielded by a large amount of dust. The amount by which dust can be processed in starburst regions is likely related to the mass and age of the starburst as well as the extent to which the dust can shield itself. Additional work on other fairly reddened starburst regions is needed to test this interpretation of the origin of the MW-type dust we find in the M33 nucleus.

5.4. Possible Role of Collisions and Mergers

The low velocity dispersion and extreme compactness of the M33 nucleus have caused Lauer et al. (1998) to suggest that stellar mergers might play an important role in creating the blue stellar population (see also Kormendy & McClure 1993). These arguments are based on a calculation that a typical star lying within the present-day environment of the M33 nucleus would have a collision/binary capture timescale of about a Hubble time. This model could apply if the previous estimate of an old (10^{10} yr) stellar population in the nucleus of M33 is assumed (Ciani, D’Odorico, & Benvenuti 1984; Schmidt et al. 1990). That is, if conditions in the nucleus have not changed over a Hubble time, most stars in the nucleus will have undergone such an event. To assess if collisions and mergers are important, we will assume the age of the nucleus is on the order of the Hubble time and see if reasonable arguments lead to the observed characteristics of the M33 nucleus.

The optical spectrum of M33 (Figure 1) demonstrates that the nucleus contains many stars of $\sim 2.5 - 6 M_{\odot}$. The observed nuclear B magnitude is 14.6. Corrected for foreground and internal dust, the intrinsic B magnitude is 12.5, corresponding to a $M_B = -12.0$ (for a distance of 795 kpc). For the purposes of this exercise, we attribute most of the nuclear mass of $5 \times 10^5 M_{\odot}$ to an

old stellar population that creates more massive stars by mergers. The absolute blue magnitude would require the presence of $\sim 10^5$ main sequence stars with masses $\sim 3 M_\odot$, if these stars were the most massive in the nucleus. This hypothetical population accounts for an uncomfortably large portion of the total nuclear mass. Instead, it seems required that the light from the nucleus is dominated by stars closer to the top of the permitted mass range ($6M_\odot$). We assume the old stellar population is described by an IMF similar to the one taken for the starburst, up to a main sequence turnoff mass of $0.9 M_\odot$. Allowing for the mass lost in mergers, stars at the turnoff must undergo on the order of six to eight mergers to build a $5 - 6 M_\odot$ star. Thus, the calculation by Lauer et al. (1998) that, on average, each star might undergo one merger in a Hubble time implies that the dominant stars could not be created in this fashion.

A more rigorous argument would account for the dynamical evolution of the nucleus. If the age of the M33 nucleus is on the order of the Hubble time, then it is possible that it has gone through core collapse (Hernquist, Hut, & Kormendy 1991; Kormendy & McClure 1993; Lauer et al. 1998). Lee (1987) has studied stellar mergers in dynamical models of systems of $0.7 M_\odot$ stars which, in their post core collapse configuration, resemble the M33 nucleus. The merger rate reaches a sharp peak around core collapse. Stars that are the result of eight mergers, as required to build the blue stars in the M33 nucleus, are 10^{-5} less common than the original population members shortly after core collapse in Lee’s (1987) model. We have roughly corrected this result for the approximately three times higher number of seed stars in M33 compared with the modeled cluster. In addition, Lee (1987) made the optimistic assumptions that all binary captures lead to mergers (rather than the expected $\sim 25\%$; Lee & Ostriker 1986) and that the merged stars have main sequence lifetimes similar to normal stars (whereas the lifetimes are shortened considerably by the presence of enriched nuclear material; e.g., Sills et al. 1997). We project that mergers would yield at best an order of magnitude less than the numbers of massive stars required. This conclusion agrees with the statement by Hernquist et al. (1991).

The merger hypothesis is attractive primarily because of the very small observed core radius in M33. However, the observations are dominated by the relatively massive stars; hence we have to examine the time scale for mass segregation to be sure that the radius measured is representative of the distribution of lower mass stars that hypothetically merge due to their high density in this core. We have estimated the dynamical decay time for stars of $5 M_\odot$ in a total mass of $1 \times 10^6 M_\odot$ distributed over a radius of 0.5 pc, assuming that the density goes as $1/r^2$, $1/r$, or is constant within this radius. The calculations are based on equation (7-18) of Binney & Tremaine (1987). We find that the dynamical decay time from formation at a radius of 0.5 pc is in all three cases substantially less than the lifetimes of the stars; that is, mass segregation is likely to have occurred. The increasing size of the nucleus with wavelength (see Table 5) and corresponding observed color gradients (Kormendy & McClure 1993; Lauer et al. 1998) confirm that the blue, massive stars have probably sunk to the center and are surrounded by a population of lower mass stars. Thus, estimates of the merger rate based on the small observed core radius (e.g., Lauer et al. 1998 and our discussion in the preceding paragraphs) are likely to be too high.

The merger hypothesis can also be tested by examining the properties of the merger products. These products have huge angular momentum compared with normal stars (e.g., Rasio & Shapiro 1995). If the interiors become convective, the resulting high rotation rates may be spun down through magnetic interaction with circumstellar disks (Leonard & Livio 1995). However, the resulting mixing of metal rich material causes the evolution of the stars to differ significantly from that of normal stars (e.g., Baily & Pinsonneault 1995; Sills et al. 1997). The possibility of abnormal stellar evolution is made very unlikely by the success in our spectral synthesis evolutionary models in fitting the properties of the nucleus across the entire spectrum, since these models assume normal evolution. The possibility that the nuclear population is characterized by abnormally high rotational velocities is contradicted by the small net velocity dispersion.

If the merger mechanism played an important role in M33, then the conclusions drawn from starburst models would largely be vitiated. However, a variety of arguments show that mergers play a negligible role and hence that the blue stellar population must arise in a starburst as described in Section 5.2.

6. Conclusions

By fitting the UV to near-IR SED of the M33 nucleus with a starburst model which includes stars, gas, and dust, we find the M33 nucleus to be composed of a ~ 70 Myr burst of star formation with a mass of $\sim 7 \times 10^5 M_{\odot}$ enshrouded by a shell of MW-type dust ($\tau_V \sim 2$). This result is different from previous work which modeled the nucleus using both young ($10^7 - 10^8$ years) and old ($10^9 - 10^{10}$ years) stellar populations subject only to modest reddening. By including the effects of dust internal to M33, we are able to reproduce the relatively red SED of the M33 nucleus without requiring a luminous old stellar population. As a result, this work is more consistent with the small size and the detection of far-UV flux from the nucleus.

The dust in M33 has a strong 2175 Å bump, in contrast to other UV-bright starbursts that do not show this feature. Not much can be said with a sample of one galaxy, but it is possible that the different dust characteristics in M33 nucleus are related to the higher optical depth of dust and/or the age of the starburst. Thus, there is not a single type of dust found in starburst galaxies but a range of types varying from that found in the MW to the SMC. Correcting for the effects of dust in starburst galaxies must be done with care, especially in the UV.

The M33 nuclear starburst resembles the ultracompact population of very massive and luminous stars in the center of the Milky Way, both in the peak luminosity deduced for the starbursts responsible and in the size of the starburst region. It seems likely that ultracompact starbursts (< 1 pc) are common in the nuclei of normal galaxies and may influence the evolution of these regions significantly.

Confirmation of our interpretation of the M33 nucleus would be greatly helped by additional UV and far-IR observations. A good UV spectrum of just the nucleus would be easily obtained by

the STIS instrument on HST due to its high sensitivity and small apertures. Far-IR observations at high spatial resolution would help put stringent constraints on the mass of the dust internal to the nucleus. These observations should be possible with SIRTf.

We thank the anonymous referee for valuable suggestions which improved the presentation of our work. This work benefited from discussions about SES models with Claus Leitherer, Michel Fioc, and Brigitte Rocca-Volmerange. In addition, we are indebted to Claus Leitherer and Michel Fioc for providing us with new grids of SEDS from the L98 and PEGASE SES models. We thank Juhan Frank for helpful discussion on the X-ray properties of binaries and the intricacies of cluster dynamics. Support for this work was provided by NASA through grant number [AR-08002.01-96A] from the Space Telescope Science Institute. Additional support was provided by the NSF under grant AST95-29190. MMH received support for this work provided by NASA through Hubble Fellowship grant #HF-1072.01-94A awarded by the Space Telescope Science Institute.

REFERENCES

- Bailyn, C. D., & Pinsonneault, M. H. 1995, *ApJ*, 439, 705
- Bessell, M. S. 1990, *PASP*, 102, 1181
- Bessell, M. S. & Brett, J. M. 1988, *PASP*, 100, 1134
- Bessell, M. S., Castelli, F., & Plez, B. 1998, *A&A*, 333, 231
- Bica, E. & Alloin D. 1986, *A&A*, 162, 21
- Bica, E. & Alloin D. 1987, *A&A*, 186, 49
- Binney, J., & Tremaine, S. 1987, "Galactic Dynamics" (Princeton Univ. Press: Princeton, N. J.), 425
- Biretta et al. 1996, *WFPC2 Instrument Handbook*, version 4.0 (Baltimore: STScI)
- Ciani, A., D'Odorico, S., & Benvenuti, P. 1984, *A&A*, 137, 223
- Calzetti, D., Kinney, A. L., & Storchi-Bergmann, T. 1994, *ApJ*, 429, 582
- Cardelli, J. A., Clayton, G. C., & Mathis, J. S. 1989, *ApJ*, 345, 245
- Cardelli, J. A. & Savage, B. D. 1988, *ApJ*, 325, 864
- Doyon, R., Joseph, R. D., & Wright, G. S. 1994, *ApJ*, 421, 101
- Dubus, G., Charles, P. A., Long, K. S., & Hakala, P. J. 1997, *ApJ*, 490, L47

- Fioc, M. & Rocca-Volmerange, B. 1997, *A&A*, 326, 950
- Fioc, M. & Rocca-Volmerange, B. 1998, in preparation
- Frogel, J. A., Persson, S. E., Aaronson, M., Matthews, K. 1978, *ApJ*, 220, 75
- Garnett, D. R., Shields, G. A., Skillman, E. D., Sagan, S. P., & Dufour, R. J. 1997, *ApJ*, 489, 63
- Gallagher, J. S., Goad, J. W., & Mould, J. 1982, *ApJ*, 263, 101
- Gordon, K. D., Calzetti, D., & Witt, A. N. 1997, *ApJ*, 487, 625
- Gordon, K. D. & Clayton, G. C. 1998, *ApJ*, 500, 816
- Gordon, K. D., Witt, A. N., & Friedmann, B. C. 1998, *ApJ*, 498, 522
- Hernquist, L., Hut, P., & Kormendy, J. 1991, *Nature*, 354, 376
- Holtzman, J., et al. 1995, *PASP*, 107, 156
- Hunt, L. K., Mannucci, F., Testi, L., Migliorini, S., Stanga, R. M., Baffa, C., Lisi, F., & Vanzi, L. 1998, *AJ*, 115, 2594
- Hunter, D. A., Light, R. M., Holtzman, J. A., Lynds, R., O’Neil, E. J., Jr., & Grillmair, C. J. 1997, *ApJ*, 478, 124
- Jones, A. P., Tielens, A. G. G. M., & Hollenbach, D. J. 1996, *ApJ*, 469, 740
- Krist, J. & Hook, R. 1997, *The Tiny Tim User’s Guide*, version 4.4 (Baltimore: STScI)
- Kormendy, J. & McClure, R. D. 1993, *AJ*, 105, 1793
- Lançon, A. & Rocca-Volmerange, B. 1992, *A&AS*, 96, 593
- Lauer, T. R., Faber, S. M., Ajhar, E. A., Grillmair, C. J., & Scowen, P. A. 1998, *AJ*, 116, 2263
- Lee, H. M. 1987, *ApJ*, 319, 801
- Lee, H. M., & Ostriker, J. P. 1986, *ApJ*, 310, 176
- Leitherer, C. & Heckman, T. M. 1995, *ApJS*, 96, 9
- Leitherer, C. et al. 1998, *ApJS*, submitted
- Lejeune, Th., Cuisinier, F., & Buser, R. 1997, *A&AS*, 125, 229
- Leonard, P. J. T., & Livio, M. 1995, *ApJ*, 447, L121
- Massey, P., Bianchi, L., Hutchings, J. B., & Stecher, T. P. 1996, *ApJ*, 469, 629

- McQuade, K., Calzetti, D., & Kinney, A. L. 1995, *ApJS*, 97, 331
- Minniti, D., Olszewski, E. W., & Rieke, M. 1993, *ApJ*, 410, L79
- Misselt, K. A., Clayton, G. C., & Gordon, K. D. 1998, *ApJ*, in press
- Monteverde, M. I., Herrero, A., Lennon, D. J., & Kurdritzki, R.-P. 1997, *ApJ*, L107
- Morgan, W. W. & Mayall, N. U. 1957, *PASP*, 69, 291
- Nichols, J. S., Garhart, M. P., De La Peña, M. D., & Levay, K. L. 1994, *New Spectral Image Processing System Information Manual: Low Dispersion Data - Version 1.0*, *IUE Newsletter* No. 53
- O’Connell, R. W. 1983, *ApJ*, 267, 80
- O’Donnell, J. E. & Mathis, J. S. 1997, *ApJ*, 479, 806
- Rasio, F. A., & Shapiro, S. L. 1995, *ApJ*, 438, 887
- Rieke, G. H. & Lebofsky, M. J. 1982, in “The Galactic Center” (*Am. Inst. of Phys.: New York*), 194
- Rieke, G. H., Loken, K., Rieke, M. J., & Tamblyn, P. 1993, *ApJ*, 412, 99
- Salpeter, E. E. 1955, *ApJ*, 121, 161
- Scalo, J. 1998, *Proceedings of Herstmonceux Conference on IMF*, in press
- Schmidt, A. A., Bica, E., & Alloin, D. 1990, *MNRAS*, 243, 620
- Schulman, E. & Bergman, J. N. 1995, *ApJ*, 441, 568
- Shier, L. M., Rieke M. J., & Rieke, G. H. 1996, *ApJ*, 470, 222
- Sills, A., Lombardi, J. C., Baily, C. D., Demarque, P., Rasio, F. A., & Shapiro, S. L. 1997, *ApJ*, 487, 290
- Stecher, T. P., et al. 1997, *PASP*, 109, 584
- Taylor, J. R. 1982, *An Introduction to Error Analysis* (Mill Valley, CA: Univ. Science Books)
- Trinchieri, G., Fabbiano, G., & Peres, G. 1988, *ApJ*, 325, 531
- van den Bergh, S. 1991, *PASP*, 103, 609
- Voit, M., et al. 1997, *HST Data Handbook, version 3.0* (Baltimore: STScI)
- Wainscoat, R. J. & Cowie, L. L. 1992, *AJ*, 103, 332

- Werner, M. W. & Davidson, J. A. 1989, in "The Center of the Galaxy" ed. M. Morris (Kluwer: Dordrecht), 423
- Whitmore, B., Heyer, I., Baggett, S. 1997, Instrument Science Report WFPC2 96-4 (Baltimore: STScI)
- Williams, D. M., Thompson, C. L., Rieke, G. H. & Montgomery, E. F. 1993, Proc. SPIE, 1946, 482
- Witt, A. N. 1977, ApJS, 35, 1
- Witt, A. N. & Gordon, K. D. 1996, ApJ, 463, 681
- Witt, A. N. & Gordon, K. D. 1998, in preparation
- Witt, A. N., Thronson, H. A., & Capuano, J. M. 1992, ApJ, 393, 611
- Zaritsky, D., Elston, R., & Hill, J. M. 1989, AJ, 97, 97